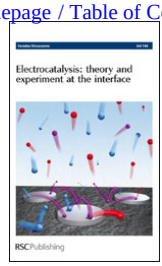

This paper is published as part of Faraday Discussions volume 140:

Electrocatalysis - Theory and Experiment at the Interface

Preface

Preface
Andrea E. Russell, *Faraday Discuss.*, 2009
DOI: 10.1039/b814058h

Introductory Lecture

Electrocatalysis: theory and experiment at the interface
Marc T. M. Koper, *Faraday Discuss.*, 2009
DOI: 10.1039/b812859f

Papers

The role of anions in surface electrochemistry
D. V. Tripkovic, D. Strmcnik, D. van der Vliet, V. Stamenkovic and N. M. Markovic, *Faraday Discuss.*, 2009
DOI: 10.1039/b803714k

From ultra-high vacuum to the electrochemical interface: X-ray scattering studies of model electrocatalysts
Christopher A. Lucas, Michael Cormack, Mark E. Gallagher, Alexander Brownrigg, Paul Thompson, Ben Fowler, Yvonne Gründer, Jerome Roy, Vojislav Stamenković and Nenad M. Marković, *Faraday Discuss.*, 2009
DOI: 10.1039/b803523g

Surface dynamics at well-defined single crystal microfacetted Pt(111) electrodes: *in situ* optical studies
Iosif Fromondi and Daniel Scherson, *Faraday Discuss.*, 2009
DOI: 10.1039/b805040f

Bridging the gap between nanoparticles and single crystal surfaces
Payam Kaghazchi, Felice C. Simeone, Khaled A. Soliman, Ludwig A. Kibler and Timo Jacob, *Faraday Discuss.*, 2009
DOI: 10.1039/b802919a

Nanoparticle catalysts with high energy surfaces and enhanced activity synthesized by electrochemical method
Zhi-You Zhou, Na Tian, Zhi-Zhong Huang, De-Jun Chen and Shi-Gang Sun, *Faraday Discuss.*, 2009
DOI: 10.1039/b803716g

Discussion

General discussion
Faraday Discuss., 2009,
DOI: 10.1039/b814699n

Papers

Differential reactivity of Cu(111) and Cu(100) during nitrate reduction in acid electrolyte
Sang-Eun Bae and Andrew A. Gewirth, *Faraday Discuss.*, 2009
DOI: 10.1039/b803088j

Molecular structure at electrode/electrolyte solution interfaces related to electrocatalysis
Hidenori Noguchi, Tsubasa Okada and Kohei Uosaki, *Faraday Discuss.*, 2009
DOI: 10.1039/b803640c

A comparative *in situ* ^{195}Pt electrochemical-NMR investigation of PtRu nanoparticles supported on diverse carbon nanomaterials
Fatang Tan, Bingchen Du, Aaron L. Danberry, In-Su Park, Yung-Eun Sung and YuYe Tong, *Faraday Discuss.*, 2009
DOI: 10.1039/b803073a

Spectroelectrochemical flow cell with temperature control for investigation of electrocatalytic systems with surface-enhanced Raman spectroscopy
Bin Ren, Xiao-Bing Lian, Jian-Feng Li, Ping-Ping Fang, Qun-Ping Lai and Zhong-Qun Tian, *Faraday Discuss.*, 2009
DOI: 10.1039/b803366h

Mesoscopic mass transport effects in electrocatalytic processes
Y. E. Seidel, A. Schneider, Z. Jusys, B. Wickman, B. Kasemo and R. J. Behm, *Faraday Discuss.*, 2009
DOI: 10.1039/b806437g

Discussion

General discussion
Faraday Discuss., 2009,
DOI: 10.1039/b814700k

Papers

On the catalysis of the hydrogen oxidation
E. Santos, Kay Pötting and W. Schmickler, *Faraday Discuss.*, 2009
DOI: 10.1039/b802253d

Hydrogen evolution on nano-particulate transition metal sulfides
Jacob Bonde, Poul G. Moses, Thomas F. Jaramillo, Jens K. Nørskov and Ib Chorkendorff, *Faraday Discuss.*, 2009
DOI: 10.1039/b803857k

Influence of water on elementary reaction steps in electrocatalysis
Yoshihiro Gohda, Sebastian Schnur and Axel Groß, *Faraday Discuss.*, 2009
DOI: 10.1039/b802270d

Co-adsorbtion of Cu and Keggin type polytungstates on polycrystalline Pt: interplay of atomic and molecular UPD
Galina Tsirlina, Elena Mishina, Elena Timofeeva, Nobuko Tanimura, Nataliya Sherstyuk, Marina Borzenko, Seiichiro Nakabayashi and Oleg Petrii, *Faraday Discuss.*, 2009
DOI: 10.1039/b802556h

Aqueous-based synthesis of ruthenium–selenium catalyst for oxygen reduction reaction
Cyril Delacôte, Arman Bonakdarpour, Christina M. Johnston, Piotr Zelenay and Andrzej Wieckowski, *Faraday Discuss.*, 2009
DOI: 10.1039/b806377j

Size and composition distribution dynamics of alloy nanoparticle electrocatalysts probed by anomalous small angle X-ray scattering (ASAXS)
Chengfei Yu, Shirlaine Koh, Jennifer E. Leisch, Michael F. Toney and Peter Strasser, *Faraday Discuss.*, 2009
DOI: 10.1039/b801586d

Discussion

General discussion
Faraday Discuss., 2009,
DOI: 10.1039/b814701a

Papers

Efficient electrocatalytic oxygen reduction by the 'blue' copper oxidase, laccase, directly attached to chemically modified carbons
Christopher F. Blanford, Carina E. Foster, Rachel S. Heath and Fraser A. Armstrong, *Faraday Discuss.*, 2009
DOI: 10.1039/b808939f

Steady state oxygen reduction and cyclic voltammetry
Jan Rossmeisl, Gustav S. Karlberg, Thomas Jaramillo and Jens K. Nørskov, *Faraday Discuss.*, 2009
DOI: 10.1039/b802129e

Intrinsic kinetic equation for oxygen reduction reaction in acidic media: the double Tafel slope and fuel cell applications
Jia X. Wang, Francisco A. Uribe, Thomas E. Springer, Junliang Zhang and Radoslav R. Adzic, *Faraday Discuss.*, 2009
DOI: 10.1039/b802218f

A first principles comparison of the mechanism and site requirements for the electrocatalytic oxidation of methanol and formic acid over Pt
Matthew Neurock, Michael Janik and Andrzej Wieckowski, *Faraday Discuss.*, 2009
DOI: 10.1039/b804591g

Surface structure effects on the electrochemical oxidation of ethanol on platinum single crystal electrodes
Flavio Colmati, Germano Tremiliosi-Filho, Ernesto R. Gonzalez, Antonio Berná, Enrique Herrero and Juan M. Feliu, *Faraday Discuss.*, 2009
DOI: 10.1039/b802160k

Electro-oxidation of ethanol and acetaldehyde on platinum single-crystal electrodes
Stanley C. S. Lai and Marc T. M. Koper, *Faraday Discuss.*, 2009
DOI: 10.1039/b803711f

Discussion

General discussion
Faraday Discuss., 2009,
DOI: 10.1039/b814702g

Concluding remarks

All dressed up, but where to go? Concluding remarks for FD 140
David J. Schiffrin, *Faraday Discuss.*, 2009
DOI: 10.1039/b816481a

Hydrogen evolution on nano-particulate transition metal sulfides†

Jacob Bonde,[a] Poul G. Moses,[b] Thomas F. Jaramillo,[c] Jens K. Nørskov[b] and Ib Chorkendorff*[a]

Received 5th March 2008, Accepted 28th March 2008
First published as an Advance Article on the web 21st August 2008
DOI: 10.1039/b803857k

The hydrogen evolution reaction (HER) on carbon supported MoS_2 nanoparticles is investigated and compared to findings with previously published work on Au(111) supported MoS_2. An investigation into MoS_2 oxidation is presented and used to quantify the surface concentration of MoS_2. Other metal sulfides with morphologies similar to MoS_2 such as WS_2, cobalt-promoted WS_2, and cobalt-promoted MoS_2 were also investigated in the search for improved HER activity. Experimental findings are compared to density functional theory (DFT) calculated values for the hydrogen binding energies (ΔG_H) on each system.

Introduction

Research efforts to develop electrocatalysts for energy conversion reactions have increased substantially in recent years. Platinum, the ubiquitous electrocatalyst used in PEM fuel cells, is both expensive and scarce, prompting widespread efforts to discover cost-effective materials to replace Pt. In this work we focus on non-noble metal sulfide catalysts for the hydrogen evolution reaction (HER) under acidic conditions, a reaction catalyzed most effectively by Pt-based materials.[1]

Previously, MoS_2 has been studied as a catalyst in hydrodesulfurisation[2] and in the photo-oxidation of organics.[3,4] In electrocatalysis, it has recently been shown that the edge structure of nanoparticulate MoS_2 is active for the HER, mimicking the active sites/co-factor of the hydrogen evolving enzymes nitrogenase and hydrogenase.[5,6] This work aims to extend the investigation on carbon-supported nanoparticulate MoS_2 for the HER. Unlike the case of Au(111) supported MoS_2 studied by STM in previous work,[6] the catalysts probed herein are more commercially relevant, which also implies that they are less homogeneous and more difficult to image on the atomic scale. As knowledge of the concentration of active sites on a catalyst surface is paramount to elucidating structure–composition–activity relationships, the first aim of this work is to utilize electrochemical oxidation to probe MoS_2 surface area, distinguishing between basal plane and edge sites. In developing this methodology to quantify active sites on a macroscopic scale, we then direct our attention to related catalyst systems, namely WS_2, cobalt-promoted WS_2, and cobalt-promoted MoS_2. We end by comparing experimentally determined activity data to predictions

[a]*Center for Individual Nanoparticle Functionality (CINF), Department of Physics, Technical University of Denmark, Lyngby, DK-2800, Denmark. E-mail: ibchork@fysik.dtu.dk*
[b]*Center for Atomic-scale Materials Design (CAMd), Department of Physics, Technical University of Denmark, Lyngby, DK-2800, Denmark*
[c]*Department of Chemical Engineering, Stanford University, 381 North-South Mall, Stauffer III, Stanford, CA 94305-5025, USA*

† The HTML version of this article has been enhanced with colour images.

made by density functional theory (DFT) models of these systems in order to gain insight into trends in catalyst activity.

It has been found that ΔG_H, the hydrogen binding energy to a given surface, is a good descriptor for identifying electrocatalyst materials with high exchange current densities.[1,7,8] A recent study[5] using DFT showed that the active sites on nitrogenase and hydrogenase bind hydrogen weakly, similar to Pt. It was also found that the overpotential of carbon supported MoS_2 is comparable to the DFT calculated hydrogen binding energy on the edge of the nanoparticles. In another study, MoS_2 nanoparticles on Au(111) were synthesized under UHV conditions, characterized by STM and examined for HER activity.[6] This study showed direct evidence that the active site of the MoS_2 nanoparticles is indeed the edge. The exchange current density was also found to be in agreement with the volcano relation between the HER exchange current density and the DFT calculated values for ΔG_H proposed by Nørskov *et al.*[7] By having identified the active site of MoS_2 particles, the next step is to modify that edge such that its ΔG_H approaches even closer to zero where the HER volcano curve has its maximum, and this is a major aim of the work presented herein.

Bulk MoS_2 consists of stacked S–Mo–S layers, and MoS_2 nanoparticles can be synthesized as single layer hexagonal structures exposing two different kinds of edges, the so-called Mo-edge and the S-edge.[9] It has been shown that the structure of nanoparticulate MoS_2 is a single layered truncated triangle primarily exposing the Mo-edge when supported on Au(111),[6,9] highly ordered pyrolytic graphite (HOPG)[10] or graphitic carbon.[11] Brorson *et al.*[11,12] also found truncated triangles by means of HAADF-STEM (high-angle annular dark-field-scanning transmission electron microscopy) in their investigation of MoS_2, WS_2 and cobalt-promoted MoS_2.

Estimating the number of active sites on a nanoparticulate catalyst is not trivial. One approach is to measure activity on well defined model systems characterized by STM, for example UHV-deposited nanoparticles[6,13] or physi- or chemisorbed molecular clusters.[14] Another option is to use a well established method to measure electrochemically active surface area such as that used with Pt based on the adsorption–desorption behavior of underpotentially deposited hydrogen, H_{upd}.[15] We note, however, that this method still relies upon the assumption that the sites active for H_{upd} are the same as those active for the HER. As we are studying metal sulfides where no such method exists, the irreversible oxidation of metal sulfides will be investigated as a measure of their surface area and edge sites.

In the following, we will show our investigation of MoS_2, WS_2 and cobalt promoted WS_2 (Co–W–S) and MoS_2 (Co–Mo–S), prepared similarly to the ones imaged by Brorson *et al.*[11] and supported on Toray carbon paper. The electrochemical measurements will be discussed in relation to DFT calculations of ΔG_H for each of the metal sulfates investigated in order to identify structure–composition–activity relationships for these systems.

Results and discussion

Synthesis and electrochemical characterization of MoS_2

MoS_2 particles on Toray carbon paper were prepared by dropping 25 μL of an aqueous ammonia heptamolybdate (1mM Mo) solution onto 1 cm^2 of Toray paper. The sample was dried in air at 140 °C followed by sulfidation in 10% H_2S in H_2 at 450 °C for 4 hours, and subsequently cooled in that same gas stream. This preparation method would typically give the highest HER current on a per gram basis; higher loadings usually led to lower HER currents.

HER activity was measured (see experimental details) and the results are plotted as Tafel (log *i*–*E*) and polarization curves (*i*–*E*) in Fig. 1. The Tafel plot exhibits a slope of 120 mV dec^{-1} and an exchange current density of 4.6×10^{-6} A $cm^{-2}_{geometric}$. Samples prepared by different methods have often yielded different Tafel slopes,

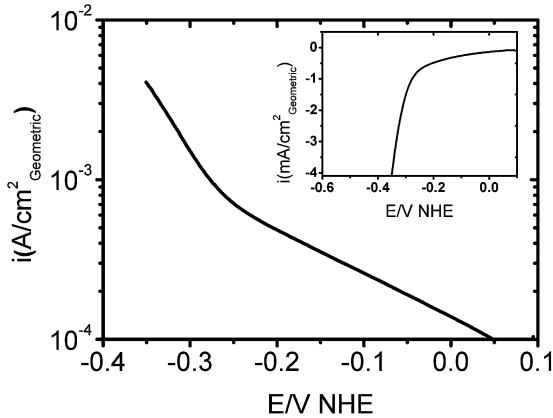

Fig. 1 Tafel plot (main) and polarization curve (inset) in the cathodic potential range of MoS_2 supported on Toray paper. The scan rate is 5 mV s^{-1} and the Tafel slope in the HER region is found to be 120 mV dec^{-1}.

ranging between 110 mV dec^{-1} and several hundred mV dec^{-1}. We attribute this to transport limitations through the fibrous, porous network characteristic of Toray carbon paper. Although sample/substrate preparation could potentially be optimized further, the consistent results achieved using the preparation method described above allows for accurate cross-comparisons among different catalyst materials. It should be noted that hydrogen evolution is taking off at around −0.2 V *vs.* NHE just as we have previously seen on MoS_2.[5,6]

The current measured from approx. +0.1 V *vs.* NHE to −0.15 V is most likely not due to the HER but rather oxygen reduction at the interface between the electrolyte and the electrode. Finally, it should be noted that sweeps between −0.35 and +0.1 V *vs.* NHE showed negligible change over time, apart from the effects of bubble formation on the electrode.

Fig. 2 shows a cyclic voltammogram of MoS_2/C where the potential is cycled between −0.3 and +1.05 V *vs.* NHE. At approx. +0.6 V *vs.* NHE an irreversible

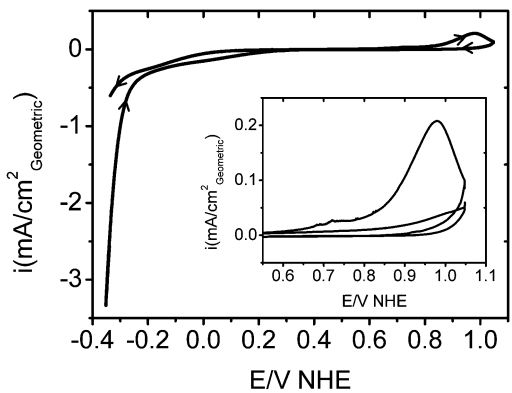

Fig. 2 Cyclic voltammogram of the oxidation and subsequent deactivation of the MoS_2 sample. Scan rate 2 mV s^{-1}. Main: the deactivation of the sample showing one sweep from −0.35 V *vs.* NHE to 1.05 V *vs.* NHE and back to −0.35 V *vs.* NHE. On the 1st anodic sweep an irreversible oxidation peak occurs at 0.6 V *vs.* NHE and is followed by a subsequent decrease in current at cathodic potentials (−0.35 V *vs.* NHE), indicating a deactivation of the active sites. Inset: the first and second sweep at anodic potentials showing a significant decrease in the oxidation peak.

oxidation begins to occur with a maximum at +0.98 V *vs.* NHE. On the subsequent cathodic sweep a significant drop in HER activity is noticed. On the ensuing anodic sweep seen in the inset of Fig. 2, the oxidation peak is no longer present. Thus, the loss of HER activity is attributed to irreversible MoS_2 oxidization. In subsequent studies, fresh samples were subjected to CVs in which an initially narrow potential window was widened gradually to more positive (anodic) potentials. It was found that the HER activity of MoS_2/C remained stable with every sweep as long as the anodic potential was limited to $\leq$+0.6 V *vs.* NHE.

MoS_2 electro-oxidation

To our knowledge, the electrochemical oxidation of nanoparticulate MoS_2 is not covered in the literature, which instead focuses on the corrosion of bulk MoS_2. Kautek and Gerischer[16] found that the bulk system preferentially oxidized at the $(10\bar{1}1)$ face and that it did not corrode at the (0001) basal plane. On the nanoparticles this would correspond to corrosion of the particle edges. Closer examination of the insert of Fig. 2 reveals two distinct oxidation peaks. The major peak has its maximum at approx. +0.98 V *vs.* NHE whereas the minor peak has its maximum at approx. +0.7 V *vs.* NHE. As the edges of MoS_2 nanoparticles are expected to be more readily oxidized than the basal plane,[16] we interpret the two distinct oxidation peaks to correspond to the edges (minor peak, +0.7 V *vs.* NHE) and the basal planes (major peak, +0.98 V *vs.* NHE) of the particles. While only one cycle to +1.05 V *vs.* NHE will completely deactivate the sample for the HER, it takes several cycles to +0.7 V *vs.* NHE to achieve the same effect. This implies that not all edge sites are oxidized with a single sweep to +0.7 V *vs.* NHE. Had the sample been deactivated for the HER after a single sweep to +0.7 V *vs.* NHE, we could definitely have used this peak as a measure of the concentration of edge sites. But as this is not the case, we will use the major peak at +0.98 V *vs.* NHE to determine the total surface area of MoS_2/C. We have however attempted to use the weak feature at +0.7 V *vs.* NHE to get an estimate of our particle size. At low sweep rates (2 mV s^{-1}), the feature is typically not dominated by the major feature at +0.98 V *vs.* NHE. The area of the edge feature is approx. 8% of the major peak. If the particles are triangular, this corresponds to an edge length of around 25 nm, consistent with the particle sizes observed by Brorson *et al.*[11]

XPS was also employed in this investigation to study the MoS_2/C at three stages of its life: freshly prepared, after HER in H_2SO_4 and after oxidation in H_2SO_4 at high anodic potentials (see experimental details). To obtain a reasonable signal to noise ratio for the XPS studies the Toray paper was dip coated in a 0.14 M Mo solution instead of dropping a known amount of solution on the surface, resulting in a higher loading of Mo than previously described (a factor of 5–10 according to the charge of the oxidation peak). The survey spectra of the different samples showed no contaminants on the freshly prepared samples. On the samples that had been submerged in H_2SO_4, peaks corresponding to sulfate were seen and a peak corresponding to N 1s was also seen. The N 1s peak is most likely caused by trace amounts of NH_3 present in air absorbed by H_2SO_4 as $(NH_4)_2SO_4$ with a N 1s binding energy of 401.3 eV.[17]

The XPS data, see Fig. 3. reveals that the freshly prepared sample (no. 1) of MoS_2 is similar to previously reported MoS_2 spectra.[18–20] The XPS data from a similarly prepared sample that was tested for the HER (sample no. 2a) by sweeping the potential between +0.1 V and −0.45 V *vs.* NHE, showed an increase in the SO_4^{2-} peak which is to be expected as the sample had been submerged in H_2SO_4. Apart from the increase in the SO_4^{2-} peak, no significant changes were found compared to the freshly prepared sample, indicating that MoS_2/C does not change significantly during the HER. After XPS analysis of sample no. 2a, it was examined for the HER again, then cycled between −0.4 V *vs.* NHE and +1.4. V *vs.* NHE and removed from the solution at −0.32 V *vs.* NHE (sample no. 2b in the XPS spectra). A significant decrease of the Mo 3d, Mo 3p, S 2s and S 2p peaks was observed and there was

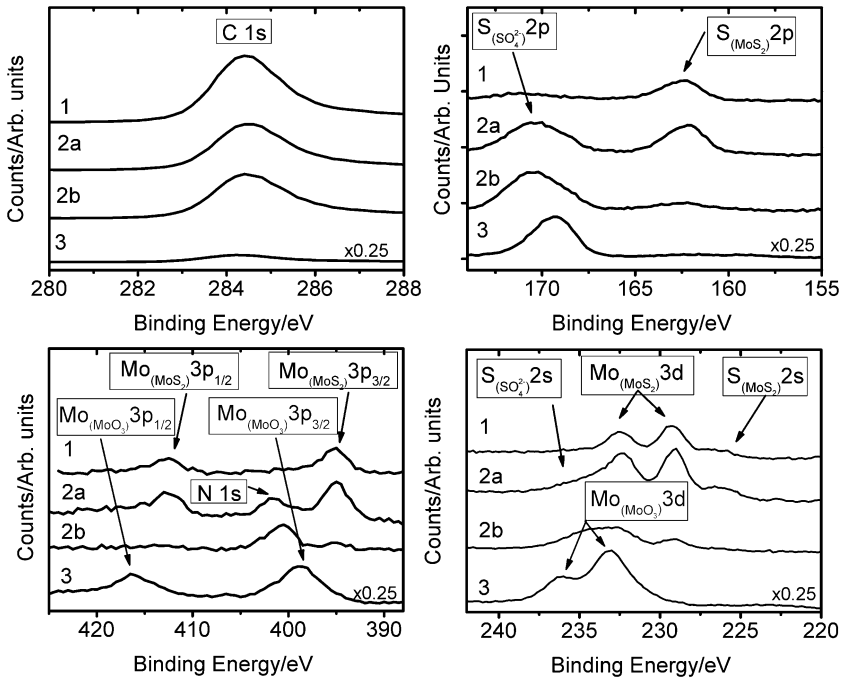

Fig. 3 XPS spectra of MoS_2 on Toray paper recorded at different stages of its life. (1) As prepared after sulfidation. (2a) After initial activity measurements of the HER (CVs between +0.1 and −0.4 V *vs.* NHE). (2b) Sample 2a after measurements of the HER and subsequent oxidation/deactivation (CVs between +1.4 and −0.4 V *vs.* NHE) and removal from the electrolyte at −0.32 V *vs.* NHE. (3) After measurements of the HER and subsequent oxidation/deactivation (CVs between +1.4 and −0.4 V *vs.* NHE) and removal from the electrolyte at 0.4 V *vs.* NHE.

no XPS signal corresponding to MoO_3. Thus, although the amount of surface Mo decreased significantly it still maintained its Mo^{4+} character (as in MoS_2). There are several possible explanations for the lack of Mo on the surface: (1) the MoS_2 desorbs from the surface at high anodic potentials, (2) the oxidation product of MoS_2, MoO_3, dissolves,[21] (3) that MoO_3 is reduced to Mo^{3+} at −0.32 V *vs.* NHE and subsequently dissolves.[21] To answer this question, sample no. 3 was subjected to the same oxidation treatment as sample no. 2b but in this case the sample was pulled out of solution at a higher potential (+0.4 V *vs.* NHE), where MoO_3 is thermodynamically stable according to the Pourbaix diagrams.[21] XPS reveals a shift of the Mo 3d and Mo 3p towards higher binding energies just as expected for MoO_3. Thus, it is unlikely that MoS_2 dissolves at anodic potentials.

We note that the Mo peaks of the MoO_3 were significantly greater than the Mo peaks observed on the other samples and at the same time the C 1s peak was significantly smaller. The increase in intensity could be due to a higher loading on this specific sample but we only found a factor of 2 larger oxidation peak on sample 3 than on sample 2a/b. This leads us to believe that there could be surface enrichment of Mo species on the outermost exposed surface of the Toray paper after repeated dissolution–redeposition cycles during each potential sweep.

Having established that the MoS_2 is in fact being oxidized at high anodic potentials we will now elaborate on possible reaction mechanisms. The reaction mechanism will enable us to use the irreversible oxidation peaks to determine the amount of MoS_2 present on the surface. A plot of the correlation between the amount of Mo used during synthesis and the charge of the irreversible oxidation

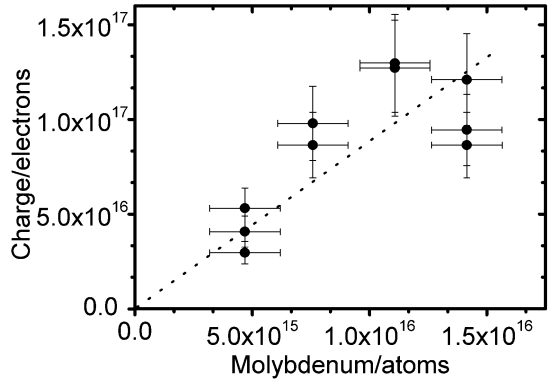

Fig. 4 The charge of the irreversible oxidation peak as a function of the amount of Mo used during the synthesis of MoS_2.

peak is shown on Fig. 4. In a corrosion study by Jaegermann and Schmeisser,[18] bulk MoS_2 was electrochemically oxidized in KNO_3 and examined by XPS. A shift toward higher binding energies was observed for the S 2p and Mo 3d peaks and a broadening was observed in the S 2p line. This was interpreted as MoS_2 degradation to SO_4^{2-}, S_2^{2-} and MoO_3. We can, with this knowledge, consider how many electrons we expect to use to oxidize one Mo atom. If we consider one extreme where the carbon supported MoS_2 is decomposed into MoO_3 and SO_4^{2-} the following reaction would take place, where 18 electrons are transferred per Mo atom:

$$MoS_2 + 11H_2O \rightarrow MoO_3 + 2SO_4^{2-} + 22H^+ + 18e^- \quad (1)$$

The other extreme would be that MoS_2 is decomposed into MoO_3 and S_2^{2-} where 4 electrons are needed:

$$MoS_2 + 3H_2O \rightarrow MoO_3 + S_2^{2-} + 6H^+ + 4e^- \quad (2)$$

According to Fig. 4, the correlation between the oxidation peak and the deposited amount of Mo yields 8.9 (r^2 =0.55) electrons per Mo atom used in the deposition. This number is in between the two extremes mentioned above. Revisiting the XPS data we can not see whether we have produced excess SO_4^{2-} due to the background of H_2SO_4. We are, however, also not seeing any significant amounts S_2^{2-} after cyclic voltammetry. While the samples have been subject to a high anodic (1.4 *vs.* NHE) potential where S_2^{2-} can be oxidized to SO_4^{2-}, the subsequent high cathodic (−0.4 *vs.* NHE) potential can reduce the S_2^{2-} to H_2S.[21] We can not conclusively determine the exact nature of the oxidation reaction. But our measurements indicate that the sulfur in the MoS_2 is only partially oxidized during anodic sweeps, resulting in the following proposed reaction mechanism:

$$MoS_2 + 7H_2O \rightarrow MoO_3 + SO_4^{2-} + \tfrac{1}{2}\, S_2^{2-} + 14\, H^+ + 11e^- \quad (3)$$

HER activity of MoS_2/C

In order to determine the activity of the MoS_2/C system per active site, we start with the irreversible oxidation to estimate the total surface area of MoS_2 on the Toray paper. The irreversible oxidation peak of the sample, shown in Fig. 1 and Fig. 2, has a charge of 0.014 C. If we assume that 11 electrons are involved in the oxidation

of MoS_2, as presented in the previous section, the surface area will be 3.8 cm^2 of single layered MoS_2 giving an exchange current density (i_0) of 1.2×10^{-6} A cm^{-2} (and a Tafel slope of 120mV dec^{-1}). We have previously shown that the active sites of Au(111) supported MoS_2 nanoparticles are situated on the edge ($i_0 = 7.9 \times 10^{-6}$ A cm^{-2}).[6]

The exchange current density on a per active site basis will clearly be higher than the exchange current densities reported above, since few of the MoS_2 sites are on the edge. Thus, the values above constitute a lower bound for activity. If we incorporate the fact that the MoS_2 nanoparticles are triangular with an edge length of 25 nm, approx. 8% of the atoms will be situated at the edge of the particle. This would lead to a 12-fold increase in exchange current density per active site.

Electrochemical characterization of WS_2

WS_2 exhibits a layered structure similar to MoS_2,[11,12] forming the same triangular shape as MoS_2 when prepared under similar conditions. WS_2 supported on SiO_2 has previously been proposed as a catalyst for the hydrogen evolution reaction.[22]

The WS_2 was studied on Toray paper and the preparation method was similar to that of the MoS_2 samples (see experimental details). In Fig. 5, the results of the electrochemical measurements are shown. Fig. 5A shows a Tafel plot (log *i*–*E*) and a polarization curve (*i*–*E*) in the region where we have previously observed hydrogen evolution on MoS_2 samples. On the polarization curve (inset of Fig. 5A) the cathodic current increases at potentials more negative than −0.2 V *vs.* NHE ascribed to HER activity. The Tafel slope on this sample is found to be 135 mV dec^{-1}, indicating that the current could be transport limited. Fig. 5b shows the deactivation of the sample at positive potentials. As with the MoS_2/C sample, an oxidation feature is observed with a peak at approx. 1 V *vs.* NHE, and on consecutive sweeps the peak disappears concurrent with a drop in the HER current. This is the same behavior as we have seen on the MoS_2/C sample except that the WS_2 sample required two sweeps towards highly anodic potentials before the HER current was affected. This behavior was also observed with high loadings of MoS_2/C samples that surely had formed multilayers. In this case, the outer layer could be passivated by a sulfur/oxide layer, thus requiring several oxidation/reduction steps to completely dissolve the metal sulfide. Apart from the potential formation of multilayers the oxidation of the WS_2 is similar to that of MoS_2/C, and it is assumed that the oxidation process is similar to that of MoS_2/C.

Cobalt promoted MoS_2 and WS_2

Cobalt is often used to promote WS_2 and MoS_2 in catalyzing the hydrodesulfurization reaction. Both the structural and the catalytic effect of adding cobalt has been extensively studied.[2] It is widely accepted that the cobalt is located at the edge of MoS_2, more specifically the so called S-edge ($\bar{1}110$). Cobalt promotion of MoS_2 has also been shown to change the morphology significantly.[11] Cobalt promoted

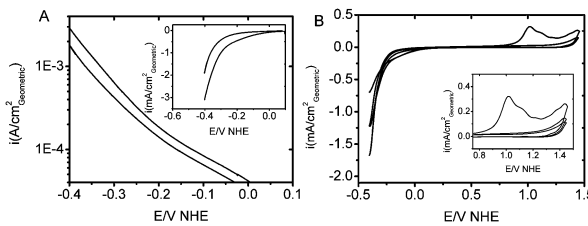

Fig. 5 A: Tafel and polarization curve (inset) of WS_2/C, scan rate 5 mV s^{-1}, both the initial and the final stable scan is shown. B: CV of WS_2/C showing the deactivation of WS_2.

MoS_2 is usually found as truncated triangles exposing the S-edge ($\bar{1}110$) predominantly, unlike the unpromoted MoS_2, in which the triangles are less truncated and primarily expose their Mo-edge ($\bar{1}010$).[23] In the following we will show data for sulfided Co and Co promoted WS_2 and MoS_2.

Electrochemical characterization of cobalt sulfide (CoS_x)

The first step in testing the promotion by cobalt is the test of sulfided cobalt itself. We have used Co(acetate) as the Co precursor as described in ref. 11. The precursor was sulfided under the same conditions as the MoS_2 and the WS_2 samples (see experimental details). The Co is expected to be in the form of Co_8S_9 immediately after sulfidation, but as this form is not stable in air,[24] our Co sulfide is most likely partially sulfided (CoS_x).

Fig. 6A shows the initial and the stable Tafel (log *i*–*E*) and polarization curves (*i*–*E*) within a narrow potential window (maximum +0.1 V *vs.* NHE). Initially the activity is high, but unlike MoS_2 and WS_2, subsequent sweeps within this potential window show a significant decrease in activity. The decrease is most likely due to the CoS_x instability in sulfuric acid, introducing ambiguity into the interpretation of the current at cathodic potentials as the HER competes with cathodic desorption or dissolution of CoS_x. In Fig. 6B a wide sweep is exhibited. The CoS_x exhibits similar oxidation features as we have seen on the MoS_2 and WS_2, but in this case the oxidation peak is shifted towards a higher potential (1.14 V *vs.* NHE). After, oxidation the HER activity drops just as with MoS_2 and WS_2, again indicating oxidation of the material.

Cobalt promoted MoS_2(Co–Mo–S) and WS_2(Co–W–S)

The Co promoted WS_2 and MoS_2 was prepared by co-impregnation of the Mo/W and the Co precursor (see experimental details). Fig. 7A and C shows the Tafel (log *i*–*E*) and the polarization (inset) curve (*i*–*E*) within a narrow potential window (maximum +0.1 V *vs.* NHE). The HER current diminishes just as on the pure CoS_x sample: it is initially high and after subsequent sweeps the current decreases noticeably, but unlike the case of pure CoS_x, remains stable at a fairly high level. This indicates that some of the Co promoter is in the state of CoS_x, but as the current stabilizes at a higher level than pure CoS_x, MoS_2 or WS_2, the remaining Co must have a promotion effect. The Tafel slopes are also in the expected region (Co–W–S 132 mV dec^{-1}, Co–Mo–S 101 mV dec^{-1}). In Fig. 7B and D, the CVs within a wide potential window are shown, and just as on the other metal sulfides we observe an irreversible oxidation peak followed by a significant decrease in HER activity. The peak maximum, however, seems to be shifted to a more anodic potential (approx. 1.1 V *vs.* NHE) than those corresponding to the unpromoted MoS_2 and WS_2.

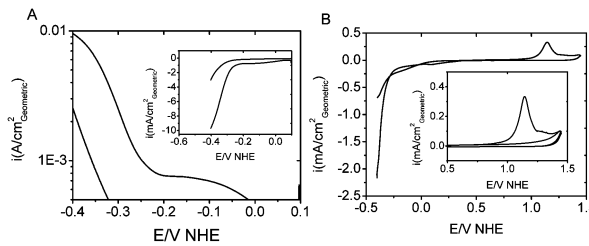

Fig. 6 A: Tafel and polarization curve (inset) of CoS_x/C, both the initial and the final stable scan is shown. B: CV of CoS_x/C showing the oxidation/deactivation of CoS_x.

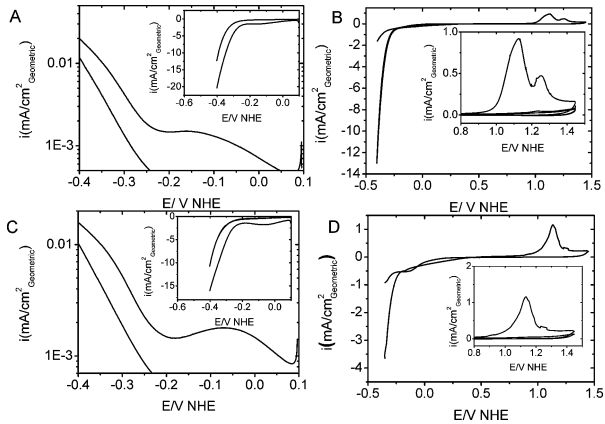

Fig. 7 A,C: Tafel and polarization curve (inset) of Co–Mo–S (A) and Co–WS (C), the scan rate is 5 mV s^{-1} both the initial and the final stable scan is shown. B,D: CV of Co–Mo–S (B) and Co–W–S (D) showing the deactivation of Co–Mo–S and Co–W–S.

DFT calculations on WS_2, MoS_2, Co–Mo–S and Co–W–S

We have calculated ΔG_H at the S-edge ($\bar{1}010$) and the Mo/W-edge ($\bar{1}010$) of WS_2 and MoS_2 and on the Co promoted S-edge ($\bar{1}010$) edge of WS_2 and MoS_2 over a wide range of S coverage and H coverage. The choice of the relevant edge configurations have been based on the chemical potential of hydrogen and sulfur at the experimental sulfiding conditions using a thermodynamic model similar to the one presented in ref. 25. The structure and the differential free energies of H adsorption for these structures can be seen in Fig. 8. The results indicate that non-promoted WS_2 and MoS_2 nanoparticles should be reasonably good hydrogen evolution catalysts, since both edges on both systems have free energies of adsorption close to zero. Hydrogen evolution on MoS_2 is expected to take place predominantly at the Mo-edge ($\Delta G_H = 0.08$ eV) rather than the S-edge ($\Delta G_H = 0.18$ eV), while for WS_2 both edges are equally good ($\Delta G_H = 0.22$ eV). Given these values for ΔG_H, non-promoted MoS_2 is predicted to be a better hydrogen evolution catalyst than WS_2.

The incorporation of cobalt into the edge structures of both WS_2 and MoS_2 is expected to have a promotion effect. The cobalt only incorporates itself into the S-edge of both cases, so ΔG_H values at the Mo/W-edge remain unaffected. At the S-edge, however, ΔG_H is reduced to 0.10 eV and 0.07 eV for MoS_2 and WS_2, respectively (down from 0.18 eV and 0.22 eV). We note that the free energy of hydrogen adsorption at the cobalt-promoted S-edge of MoS_2 is very similar to the free energy

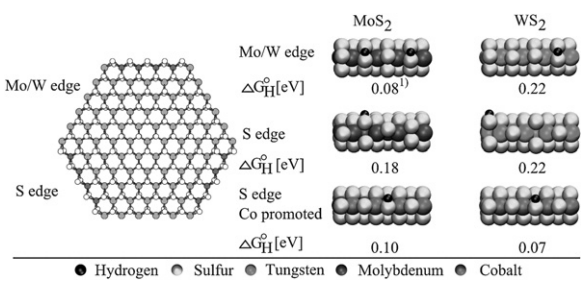

Fig. 8 Left: ball model of a Mo/WS_2 particle exposing both S-edge and Mo/W-edge. Right: differential free energies of hydrogen adsorption. 1 from ref. 5.

of hydrogen adsorption on the Mo-edge of MoS_2. Therefore, for MoS_2 the effect of promotion is the increase in the number of sites with high activity. On WS_2, the effect of cobalt promotion is the creation of new sites with higher activity than that prior to promotion.

In comparing all catalyst systems, DFT calculations suggest that cobalt-promoted MoS_2 (Co–Mo–S) should be a better catalyst than Co promoted WS_2 (Co–W–S) because it would have active sites on both edges and therefore a higher total number of active sites.

Linking catalyst structure and composition to HER activity

Calculated DFT values are best compared to experimental data where the activity has been normalized with respect to the number of active sites on the catalyst, in this case the number and type of edge sites on the different metal sulfides. We accomplish this normalization by using the irreversible oxidation features of each sulfide.

Fig. 9 exhibits normalized polarization curves (*E–i*) pertaining to each of the different samples. There is an apparent promotion effect of Co on both the MoS_2 and the WS_2 samples. The promotion effect on the WS_2 sample can be explained by the DFT calculations predicting that the Co promotion should decrease the free energy of hydrogen adsorption from 0.22 eV to 0.07 eV on the S-edge, and thus effectively increasing the activity of the active site. MoS_2 is a slightly different case. It has previously been found that the Mo-edge of MoS_2, which has a ΔG_H of 0.08 eV, is the major edge exposed, and that this edge does not adsorb cobalt.[23,26,27] However, the inhomogenous nature of these nanoparticulate catalysts suggests that both the Mo-edge and the S-edge will be present in significant fractions. Thus, the cobalt on the S-edge of MoS_2 promotes the HER, as its free energy of hydrogen adsorption is decreased from 0.18 eV to 0.10 eV. In other words, the number of active sites is increased since the normally less active S-edges becomes more active in the presence of cobalt.

Experimental and calculation details

Toray carbon paper was used as support material because it is inert, of high purity, has high conductivity and because it has adsorption sites/defects that will anchor the metal sulfide particles. The Toray paper was cut into strips that were 1 cm wide and 5 cm long. The Toray paper was loaded with catalyst by wetness impregnation with an aqueous solution of $(NH_4)_6Mo_7O_{24}\cdot 4H_2O$ in the case of MoS_2 and an aqueous solution of $H_{24}N_6O_{39}W_{12}\cdot xH_2O$ in the case of WS_2. In the case of the sulfided Co, $C_4H_4CoO_4\cdot 4H_2O$ in an aqueous solution was used. The promoted WS_2 and MoS_2 were made by co-impregnation of Co and Mo/W. The impregnation of the pure sulfides was done by dropping a 25 μL aliquot (0.3–1 mM for Mo, 0.8 mM for W, 4mM for Co). The co-impregnation of the promoted sulfides was done by

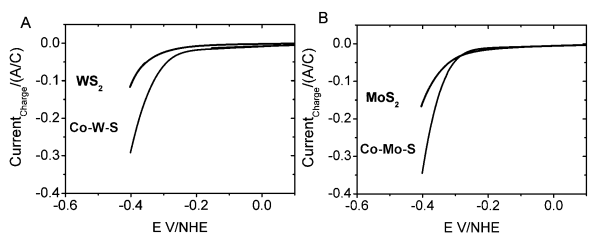

Fig. 9 Polarization curves where the currents of the different metal sulfides have been normalized with respect to the charge of the irreversible oxidation peak. A: Polarization curve of the HER on WS_2 and cobalt promoted WS_2(Co–W–S). B: Polarization curve of the HER on MoS_2 and cobalt promoted MoS_2(Co–Mo–S).

adding a 25 μL aliquot of Mo (0.7 mM) or W (0.8 mM) solution followed by a 25 μL aliquot of Co (4 mM) solution. A different sample preparation was used for the MoS_2 sample for XPS analysis where a the Toray paper was dip coated in the Mo solution (0.14 M) to obtain a more uniform impregnation.

The samples were dried at 140 °C and afterwards sulfided in a tube furnace under 10% H_2S in H_2 at 450 °C for 4 hours. The samples were cooled down in the same gas stream.

The electrochemical measurements where performed in N_2 purged 0.5 M H_2SO_4 (pH 0.4). To avoid contamination from the SCE reference electrode, a salt bridge was used. A Pt mesh was used as the counter electrode.

The XPS data was recorded using a Perkin-Elmer surface analysis system (Physical Electronics Industries Inc., USA) with a chamber base pressure of 10^{-10} Torr.

Al-Kα radiation (1486.6 eV) was used for excitation. The XPS scans on Fig. 4 were measured with a pass energy of 100 eV, a step size of 1 eV, and 250 ms $step^{-1}$.

DFT calculations

An infinite stripe model, which has previously been proven successful to investigate MoS_2 based systems,[5,28–30] is used to investigate the edges of MoS_2. The infinite stripe exposes both the $(\bar{1}010)$ Mo-edge and the $(\bar{1}110)$ S-edge. The supercell has 4 Mo atoms in the *x*-direction and 4 Mo atoms in the *y*-direction, in order to allow for important reconstructions with a period of 2 in the *x*-direction and to allow decoupling of the Mo-edge and the S-edge in the *y*-direction. The stripes are separated by 14.8 Å in the *z*-direction and 9 Å in the *y*-direction.

The plane wave density functional theory code DACAPO[31,32] is used to perform the DFT calculations. The Brillouin zone is sampled using a Monkhorst–Pack k-point set[33] containing 4 k-points in the *x*-direction and 1 k-point in the *y*- and *z*-direction. The calculated equilibrium lattice constant is 3.235 Å and 3.214 Å for MoS_2 and WS_2, respectively. A plane-wave cutoff of 30 Rydberg and a density wave cutoff of 45 Rydberg are employed using the double-grid technique.[34] Ultrasoft pseudopotentials are used except for sulfur, where a soft pseudopotential is employed.[35,36] A Fermi temperature of $k_BT = 0.1$ eV is used for all calculations and energies are extrapolated to zero electronic temperature. The exchange correlation functional RPBE is used. The convergence criterion for the atomic relaxation is that the norm of the total force should be smaller than 0.15 eV $Å^{-1}$, which corresponds approximately to a max. force on one atom below 0.05 eV $Å^{-1}$. Figures of atomic structures have been made using VMD.[37]

The differential free energies are calculated as described in ref. 5, where 0.29 eV is added to the pure DFT energy of adsorption in order to take zero point energy and entropy into account.

Conclusions

We have studied the hydrogen evolution on Co promoted and unpromoted nanoparticulate MoS_2 and WS_2 structures. Cyclic voltammetry revealed that they are irreversibly oxidized at high anodic potentials. We have used the irreversible oxidation features to determine the surface area of MoS_2 and proposed a possible oxidation mechanism of MoS_2. XPS analysis showed no change in the oxidation state of MoS_2 after HER measurements; but after oxidation at potentials above 0.6 V *vs.* NHE, MoS_2 was oxidized. We found that the activity of the carbon supported MoS_2 is comparable to that of our previously published results on Au(111) supported MoS_2. WS_2 has a similar structure and was also investigated in this study. It was found to irreversibly oxidize at high anodic potentials, just like MoS_2, and was found to be almost as active. Tests of cobalt promoted MoS_2 and WS_2 samples were also performed and Co is indeed promoting the HER in both cases. The

findings are corroborated by DFT calculations showing that the activity of the different samples should be $WS_2 < MoS_2 = Co–Mo–S < Co–W–S$.

Acknowledgements

J.B. acknowledges support from the Danish Strategic Research Council. T.F.J. acknowledge H. C. Ørsted Postdoctoral Fellowships from the Technical University of Denmark. The Center for Atomic-scale Materials Design is supported by the Lundbeck Foundation. We thank the Danish Center for Scientific Computing for computer time. The Center for Individual Nanoparticle Functionality is supported by the Danish National Research Foundation.

References

1 J. Greeley, T. F. Jaramillo, J. Bonde, I. B. Chorkendorff and J. K. Nørskov, *Nat. Mater.*, 2006, **5**, 909–913.
2 H. Topsøe, B. S. Clausen and F. E. Massoth, *Hydrotreating Catalysis*, Springer-Verlag, Berlin, 1996.
3 H. Tributsch, *Z. Naturforsch., A: Phys., Phys. Chem., Kosmophys.*, 1977, **32**, 972–985.
4 J. P. Wilcoxon, *J. Phys. Chem. B*, 2000, **104**, 7334–7343.
5 B. Hinnemann, P. G. Moses, J. Bonde, K. P. Jorgensen, J. H. Nielsen, S. Horch, I. Chorkendorff and J. K. Nørskov, *J. Am. Chem. Soc.*, 2005, **127**, 5308–5309.
6 T. F. Jaramillo, K. P. Jørgensen, J. Bonde, J. H. Nielsen, S. Horch and I. Chorkendorff, *Science*, 2007, **316**, 100–101.
7 J. K. Nørskov, T. Bligaard, A. Logadottir, J. R. Kitchin, J. G. Chen, S. Pandelov and U. Stimming, *J. Electrochem. Soc.*, 2005, **152**, J23.
8 J. Greeley, J. K. Nørskov, L. A. Kibler, A. M. El-Aziz and D. M. Kolb, *ChemPhysChem*, 2006, **7**, 1032–1035.
9 S. Helveg, J. V. Lauritsen, E. Lægsgaard, I. Stensgaard, J. K. Nørskov, B. S. Clausen, H. Topsøe and F. Besenbacher, *Phys. Rev. Lett.*, 2000, **84**, 951–954.
10 J. Kibsgaard, J. V. Lauritsen, E. Laegsgaard, B. S. Clausen, H. Topsoe and F. Besenbacher, *J. Am. Chem. Soc.*, 2006, **128**, 13950–13958.
11 M. Brorson, A. Carlsson and H. Topsøe, *Catal. Today*, 2007, **123**, 31–36.
12 A. Carlsson, M. Brorson and H. Topsøe, *J. Catal.*, 2004, **227**, 530–536.
13 J. Meier, K. A. Friedrich and U. Stimming, *Faraday Discuss.*, 2002, **121**, 365–372.
14 T. F. Jaramillo, J. Zhang, B. L. Ooi, J. Bonde, K. Andersson, J. Ulstrup, J. K. Nørskov and I. Chorkendorff, *J. Phys. Chem. C*, 2008, in press.
15 N. M. Markovic and P. N. Ross, *Surf. Sci. Rep.*, 2002, **45**, 121–229.
16 W. Kautek and H. Gerischer, *Surf. Sci.*, 1982, **119**, 46–60.
17 C. D. Wagner, A. V. Naumkin, A. Kraut-Vass, J. W. Allison, C. J. Powerll and J. R. Rumble, Jr, NIST X-Ray Photoelectron Spectroscopy Database, Standard Reference Database 20, Version 3.4, 2008, http://srdata.nist.gov/xps.
18 W. Jaegermann and D. Schmeisser, *Surf. Sci.*, 1986, **165**, 143–160.
19 T. Weber, J. C. Muijsers, H. J. M. C. van Wolput, C. P. J. Verhagen and J. W. Niemantsverdriet, *J. Phys. Chem.*, 1996, **100**, 14144–14150.
20 J. H. Nielsen, K. P. Jørgensen, J. Bonde, K. Nielsen, L. Bech, Y. Tison, S. Horch, T. F. Jaramillo and I. Chorkendorff, 2008, in preparation .
21 M. Pourbaix, Atlas of Electrochemical Equilibria, 1966.
22 A. Sobczynski, A. Yildiz, A. J. Bard, A. Campion, M. A. Fox, T. Mallouk, S. E. Webber and J. M. White, *J. Phys. Chem.*, 1988, **92**, 2311–2315.
23 J. V. Lauritsen, J. Kibsgaard, G. H. Olesen, P. G. Moses, B. Hinnemann, S. Helveg, J. K. Nørskov, B. S. Clausen, H. Topsøe, E. Lægsgaard and F. Besenbacher, *J. Catal.*, 2007, **249**, 220–233.
24 I. Alstrup, I. Chorkendorff, R. Candia, B. S. Clausen and H. Topsøe, *J. Catal.*, 1982, **77**, 397–409.
25 M. V. Bollinger, K. W. Jacobsen and J. K. Nørskov, *Phys. Rev. B: Condens. Matter Mater. Phys.*, 2003, **67**, 085410.
26 P. Raybaud, J. Hafner, G. Kresse, S. Kasztelan and H. Toulhoat, *J. Catal.*, 2000, **190**, 128–143.
27 H. Schweiger, P. Raybaud and H. Toulhoat, *J. Catal.*, 2002, **212**, 33–38.
28 B. Hinnemann, J. K. Nørskov and H. Topsøe, *J. Phys. Chem. B*, 2005, **109**, 2245–2253.

29 J. V. Lauritsen, M. Nyberg, R. T. Vang, M. V. Bollinger, B. S. Clausen, H. Topsøe, K. W. Jacobsen, E. Lægsgaard, J. K. Nørskov and F. Besenbacher, *Nanotechnology*, 2003, **14**, 385–389.
30 L. S. Byskov, J. K. Nørskov, B. S. Clausen and H. Topsøe, *J. Catal.*, 1999, **187**, 109–122.
31 S. R. Bahn and K. W. Jacobsen, *Comput. Sci. Eng.*, 2002, **4**, 56–66.
32 B. Hammer, L. B. Hansen and J. K. Nørskov, *Phys. Rev. B: Condens. Matter Mater. Phys.*, 1999, **59**, 7413–7421.
33 H. J. Monkhorst and J. D. Pack, *Phys. Rev. B: Solid State*, 1976, **13**, 5188–5192.
34 K. Laasonen, A. Pasquarello, R. Car, C. Lee and D. Vanderblit, *Phys. Rev. B: Condens. Matter Mater. Phys.*, 1993, **47**, 10142–10153.
35 N. Troullier and J. L. Martins, *Phys. Rev. B: Condens. Matter Mater. Phys.*, 1991, **43**, 1993–2006.
36 D. Vanderbilt, *Phys. Rev. B: Condens. Matter Mater. Phys.*, 1990, **41**, 7892–7895.
37 W. Humphrey, A. Dalke and K. Schulten, *J. Mol. Graphics*, 1996, **14**, 33.